Pushing revisited: Differential flatness, trajectory planning and stabilization

Jiaji Zhou and Matthew T. Mason

Abstract

We prove that quasi-static pushing with a sticking contact and ellipsoid approximation of the limit surface is differentially flat. Both graphical and algebraic derivations are given. A major conclusion is the pusher-slider system is reducible to the Dubins car problem where the sticking contact constraints translate to bounded curvature. Planning is as easy as computing Dubins curves with the additional benefit of time-optimality. For trajectory stabilization, we design closed-loop control using dynamic feedback linearization or open-loop control using two contact points as a form of mechanical feedback. We conduct robotic experiments using objects with different pressure distributions, shape, contact materials and placed at different initial poses that require difficult maneuvers to the goal pose. The average error is within 1.67mm in translation and 0.5 degrees in orientation over 60 experimental trials. We also show an example of pushing among obstacles using a RRT planner with exact steering.

1 Introduction

Robots can increase dexterity by harnessing task mechanics including inertia force, gravity and external contacts. Pushing is an example of using the arm motion and supporting surface to change the planar pose of objects through sliding. The quasi-static pusher-slider system is a canonical hybrid system with model uncertainty due to indeterminate and stochastic friction distribution. In this paper, we mainly focus on pushing with rolling/sticking contact where the object is constrained to a two

Jiaji Zhou
Robotics Institute, Carnegie Mellon University e-mail: `jiajiz@cs.cmu.edu`

Matthew T. Mason
Robotics Institute, Carnegie Mellon University e-mail: `matt.mason@cs.cmu.edu`

dimensional space embedded in SE(2). The nonholonomic constraint appears to be challenging but is fortunately not. Intuitively, the applied force through the contact point is bounded inside the friction cone and hence the turning rate of the object must be bounded, indicating similarity to the steering car system with bounded front wheel turning angle.

We use differential flatness techniques from nonlinear control theory [19], which offers some advantage for trajectory generation and control of underactuated mechanical systems. A particular interesting system is the kinematic steering car whose flat output is the center of the rear axle. The problem is well-studied: the time-optimal motion planning solution is given by Dubins curve [7] and globally stable controller sythesized with dynamic feedback linearization [21]. In this paper, we show that the pusher-slider system with single sticking contact is differentially flat, which opens a new avenue for trajectory planning and stabilization. We first give an intuitive graphical analysis and continue with an algebraic derivation.

The literature has addressed inherent model uncertainty in sliding manipulation, often in the form of worst-case guarantee. The first result is the Voting Theorem [18] that dictates the sense of rotation given a single contact knowing only the center of pressure without the exact distribution. Tighter bounds on the possible instantaneous motion are given in [22, 13]. Goyal et al. [10] noted that all the possible static and sliding frictional wrenches form a convex set whose boundary is called as the limit surface. Howe and Cutkosky [12] proposed using ellipsoid approximation of the limit surface for a given pressure distribution. Zhou et al. [27, 26] proposed a framework of representing limit surfaces using homogeneous even-degree convex polynomials. A purely data-driven method is presented in [2]. The use of multiple contacts can be open-loop stable. Lynch and Mason [17] give results on controllability and stability for open loop edge pushing. A discretized search-based planner is also given in [17]. The multiple constraints imposed by an edge can reduce uncertainty. Examples include push-grasps [3, 6], squeezing [28, 8] and parts feeding [25].

Lynch et al. [16] achieves stable translation through a round finger with only tactile sensing that gives the contact point position and normal feedback. Hogan and Rodriguez [11] recently proposed using online hybrid model predictive control for tracking a pushing trajectory. The contact modes are treated as integer variables. To avoid excessive combinatorial mode enumeration, prescribed phases of sequence with a single mode are used. Trajectory optimization and local feedback control synthesis through rigid body contacts with complementarity constraints are studied in [23, 24].

2 Background on Quasi-static Pushing

We describe the single point pusher quasi-static motion model assuming rigid body mechanics with Coulomb friction. The following notations are used:

- **q**: the object pose (x, y, θ) in the world frame W.

- **p**: the contact point (p_x, p_y) in the local frame O.
- $\mathbf{n_p}$: the inward normal in the local frame at **p**.
- **f**: the applied force by the pusher.
- $\mathbf{f_l}, \mathbf{f_r}$: the left and right edges of the friction cone.
- **u**: the pushing velocity of the pusher in the object local frame O.
- $\mathbf{u_l}, \mathbf{u_r}$: the left and right edges of the motion cone.
- **F**, **V**: the applied wrench and resultant twist in the object local frame.

The force-motion model for quasi-static pushing given certain pressure distribution can be efficiently established through limit surface representation [9, 27, 12]. Points inside the surface correspond to static friction wrenches. Points on the surface correspond to friction wrenches with normals parallel to sliding twist directions, forming a mapping between friction wrench and sliding twist.

Using a homogeneous even-degree convex polynomial $H(\mathbf{F})$ representation for the limit surface [27], the resultant object twist V follows the same direction as the gradient evaluated at the applied wrench **F**:

$$\mathbf{V} = k\nabla H(\mathbf{F}), \qquad k > 0, \tag{1}$$

A global diagonal ellipsoid approximation [16, 11] is often adopted as a convenient representation by existing literature on model-based pushing, i.e., assuming $H(\mathbf{F}) = \mathbf{F}^T A \mathbf{F}$, where $A = \mathrm{diag}([a, a, b])$. In this paper, we find the closest vector of form $[a, a, b]^T$ to the diagonal vector of $\nabla^2 H(\mathbf{F_{n_p}})$ as a local approximation, where $\mathbf{F_{n_p}}$ is the normal contact wrench at the contact point **p**, i.e., the wrench applied as if the contact is frictionless.

$$a = (\nabla^2 H(\mathbf{F}_{n_p})_{11} + \nabla^2 H(\mathbf{F}_{n_p})_{22})/2 \tag{2}$$
$$b = \nabla^2 H(\mathbf{F}_{n_p})_{33} \tag{3}$$

Choose the positive y axis of the local body frame to align with the vector pointing from the contact point to the center of mass O. In doing so, $p_x = 0$. After absorbing the scalar k into **f**, we have that in local frame

$$\mathbf{V_x} = af_x \tag{4}$$
$$\mathbf{V_y} = af_y \tag{5}$$
$$\mathbf{V_\theta} = b\tau = -bp_y f_x. \tag{6}$$

The quasi-static motion equations in global frame are written as:

$$\dot{x} = a(f_x \cos\theta - f_y \sin\theta) \tag{7}$$
$$\dot{y} = a(f_x \sin\theta + f_y \cos\theta) \tag{8}$$
$$\dot{\theta} = -bp_y f_x, \tag{9}$$

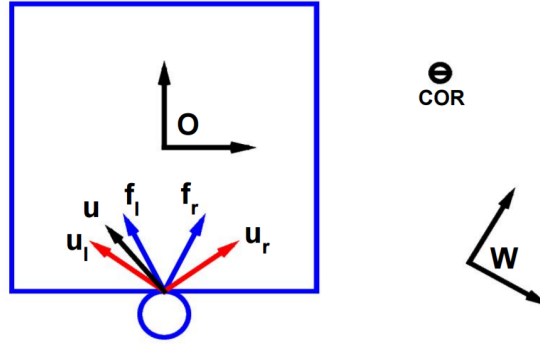and the friction cone constraint is given by

Fig. 1: A rectangle pushed by a round finger. Blue arrows correspond to the friction cone $\mathcal{K}(f_l, f_r)$ edges and red arrows correspond to the motion cone $\mathcal{K}(u_l, u_r)$ edges. The instantaneous clockwise center of rotation is marked as a circle with negative sign. The contact sticks since the pushing direction u is inside the motion cone.

$$\|f_x\| \leq \mu f_y \tag{10}$$

$$f_y \geq 0 \tag{11}$$

Denote by $J_p = \begin{bmatrix} 1 & 0 & -p_y \\ 0 & 1 & p_x \end{bmatrix}$ the Jacobian matrix at $\mathbf{p}$ and $R(\theta) = \begin{bmatrix} \cos\theta & -\sin\theta & 0 \\ \sin\theta & \cos\theta & 0 \\ 0 & 0 & 1 \end{bmatrix}$,

equations 7-9 is equivalent to:

$$\dot{\mathbf{q}} = R(\theta) A J_p^T \mathbf{f} \tag{12}$$

Note that the magnitude of $\mathbf{f}$ does not have physical meaning and is proportional to the magnitude of the input velocity. Since the pusher is position controlled, we will need to relate the applied force to pushing velocity. It can be shown [26] that for sticking contact the applied force $\mathbf{f}$ and pushing velocity $\mathbf{u}$ are linearly related, and have a one-to-one mapping:

$$\mathbf{u} = J_p A J_p^T \mathbf{f}. \tag{13}$$

Further, the friction cone constraint is translated into motion cone $\mathcal{K}(\mathbf{u_l}, \mathbf{u_r})$ where the left edge $\mathbf{u_l}$ and right edge $\mathbf{u_r}$ of the cone are given by:

$$\mathbf{u}_l = J_p A J_p^T \mathbf{f_l}, \qquad \mathbf{u}_r = J_p A J_p^T \mathbf{f_r}. \tag{14}$$

If $\mathbf{u}$ is within the motion cone, then the contact sticks as shown in Fig. 1. Left sliding occurs if $\mathbf{u}$ is to the left of $\mathbf{u_l}$ and right sliding occurs if $\mathbf{u}$ is to the right of $\mathbf{u_r}$. The planner and controller described in the rest of the paper assumes the control input is applied force, which will be converted to pusher velocity using equation 13.

3 Differential Flatness

The rough idea of differential flatness is to find flat output states (of the same dimension as control input) as a function of the original states and control inputs. Such mapping also admits an inverse function such that the original states and control inputs can be recovered from the flat output states and their high order derivatives without any integration step.

3.1 Graphical Derivation

From equations 4-6, an applied body wrench $\mathbf{F} = [\mathbf{f_x}, \mathbf{f_y}, \tau]$ is mapped to a body twist V. A twist in a plane can be further represented as a center of rotation $(\mathbf{V_x}/\mathbf{V}_\theta, \mathbf{V_y}/\mathbf{V}_\theta)$ with the same sign as $\mathbf{V}_\theta$. Let $r = |p_y|$ be the distance from the line of force to the local frame origin. The distance $\tilde{r}$ from the center of rotation (COR) to the origin is inverse proportion to r:

$$\tilde{r} = \sqrt{\frac{\mathbf{V_x^2} + \mathbf{V_y^2}}{\mathbf{V}_\theta^2}} = \frac{a}{br}. \tag{15}$$

If we define the unit length as a/b, then the COR lies on the opposite side along the perpendicular line to the line of force through the contact point, with distance to the origin equals $1/r$. As in projective geometry, the dual of a line is a point. Here, the line of applied force is mapped to the resultant COR point.

Proposition 1. *The instantaneous rotation centers corresponding to applied frictional forces through the contact point form a line perpendicular to the vector from the origin to the contact point. The distance from the line to the origin equals $\frac{a}{br}$, where r is the distance from the contact point to the origin.*

This is similar to the force-dual method [4] that maps a line of force to the acceleration center. The matrix A can be treated as a damping matrix that relates force to velocity, analogous to the inertia matrix in [4] that maps force to acceleration.

In Figure 2a, the friction cone is symmetric with respect to the origin as the contact point's normal passes through the origin. The friction cone constraints are represented using the force dual graphical method. Denote by z_l and z_r the instantaneous rotation centers given applied forces on the left edge f_l and the right edge f_r of the friction cone respectively. The allowable motion of z can be characterized by a ray (blue) of counter-clockwise rotation center starting from z_r or a ray (magenta) of clockwise rotation center starting from z_l. Figure 2b illustrates the general asymmetric case. Choose the positive y axis to be aligned with the vector pointing from the contact point to the center of mass, the trajectory of the pushed object can be exactly recovered from the trajectory of such point (flat output).

Theorem 1. *Any point on the line of center of rotations is a differentially flat output.*

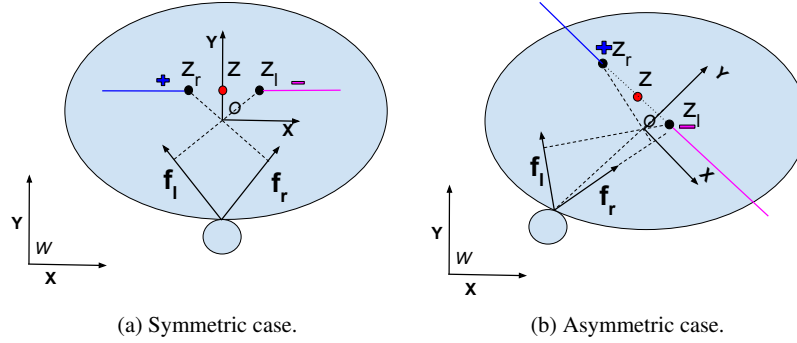(a) Symmetric case.   (b) Asymmetric case.

Fig. 2: Graphical analysis.

Proof. Section 3.2 provides an algebraic proof. We also give a geometrical proof sketch here.

1. Since the line of CORs is perpendicular to the positive y axis, the tangents along the trajectory point in the directions of body positive y axis (heading) of the object.
2. After knowing the orientation of the body frame, we can compute the position of the body frame since the point is fixed in the body frame.
3. The instantaneous COR can be further determined from the curvature along the trajectory. Therefore the velocity control input is also known.

A key observation is that if we choose the mid point (in red) between z_l and z_r, then the instantaneous motion constraints from the sticking contact are simply minimum turning radius constraints. We now have a reduction to a Dubins car model [14, 7] where the heading aligns with the positive body y axis and the mid point (red) of z_l and z_r is the center of rear axle.

3.2 Algebraic Derivation

This section derives the function mappings between cartesian pose and control to flat outputs.

3.2.1 Symmetric Case

The symmetric case as shown in Figure 2a is when the pushing point's normal aligns with the vector pointing from the point p to the center of mass O. Hence we have $p_x = 0$ and $r = -p_y$. $\cos\theta \times (7) + \sin\theta \times (8)$ and $-\sin\theta \times (7) + \cos\theta \times (8)$ yield

$$f_x = \frac{1}{a}(\dot{x}\cos\theta + \dot{y}\sin\theta) \tag{16}$$

$$f_y = \frac{1}{a}(-\dot{x}\sin\theta + \dot{y}\cos\theta). \tag{17}$$

Together with equation (9) yields

$$-\frac{a}{br}\dot{\theta} + \dot{x}\cos\theta + \dot{y}\sin\theta = 0. \tag{18}$$

A choice of flat outputs are given by

$$z_1 = x - \frac{a}{br}\sin\theta \tag{19}$$

$$z_2 = y + \frac{a}{br}\cos\theta, \tag{20}$$

whose derivative are

$$\dot{z}_1 = \dot{x} - \frac{a}{br}\cos\theta\,\dot{\theta} \tag{21}$$

$$\dot{z}_2 = \dot{y} - \frac{a}{br}\sin\theta\,\dot{\theta} \tag{22}$$

Rewrite equation (18) using $z, \dot{z}$ we get

$$\dot{z}_1\cos\theta + \dot{z}_2\sin\theta = 0. \tag{23}$$

Therefore,

$$\theta = \arctan\left(\frac{-\dot{z}_1}{\dot{z}_2}\right) \tag{24}$$

$$x = z_1 - \frac{a\dot{z}_1}{br\sqrt{\dot{z}_1^2 + \dot{z}_2^2}} \tag{25}$$

$$y = z_2 - \frac{a\dot{z}_2}{br\sqrt{\dot{z}_1^2 + \dot{z}_2^2}} \tag{26}$$

$$f_x = \frac{\dot{z}_1\ddot{z}_2 - \dot{z}_2\ddot{z}_1}{br(\dot{z}_1^2 + \dot{z}_2^2)} \tag{27}$$

$$f_y = \frac{\sqrt{\dot{z}_1^2 + \dot{z}_2^2}}{a} \tag{28}$$

The friction cone constraints represented in flat output space can be written as

$$\left|\frac{\dot{z}_1\ddot{z}_2 - \dot{z}_2\ddot{z}_1}{(\dot{z}_1^2 + \dot{z}_2^2)^{\frac{3}{2}}}\right| \leq \frac{br\mu}{a} \tag{29}$$

Note that constraints (29) is exactly the curvature of the trajectory of $z(t)$. We can now conclude that pushing with sticking constraint is equivalent to finding curves with bounded curvature that connects two 2D oriented points. In particular, Dubins curve [7] is the time-optimal solution.

Figure 3 demonstrate two examples of trajectory planning with a single point sticking contact. The friction cone constraint is converted to minimum turning radius constraint. Dubins curve is generated in flat output space. Then the SE(2) poses of the object and control actions are mapped back to the cartesian space as given in equations 24 and 25-28.
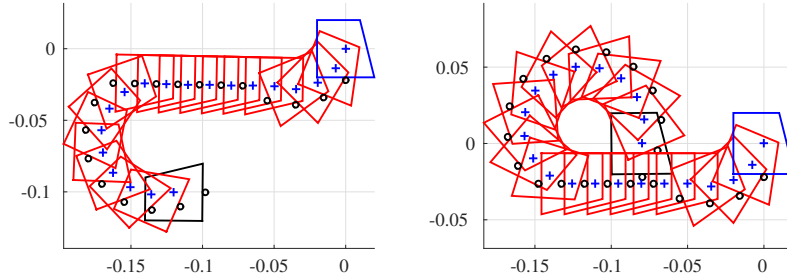
Fig. 3: Example planned trajectories with the initial pose in black and the final pose in blue.

3.2.2 General Case

We also derive the general case when the contact point's normal is not aligned with the the vector as shown in Figure 2b. Let the local frame origin be the COM and the positive y-axis aligned with the vector pointing from the contact point p to center of mass O. We show that with this choice of reference frame, any point on the dual line of the friction cone is differentially flat, and conveniently we can simply choose the mid point between the two extreme CORs that correspond to left and right edges of the friction cone. Denote by c_x the x component along the line of CORs, and $\rho = \frac{a}{b}$. The flat outputs are given by

$$
\begin{bmatrix} z_1 \\ z_2 \end{bmatrix} = \begin{bmatrix} x \\ y \end{bmatrix} + \begin{bmatrix} \cos\theta & -\sin\theta \\ \sin\theta & \cos\theta \end{bmatrix} \begin{bmatrix} c \\ \rho/r \end{bmatrix},
\tag{30}
$$

where the vector $\begin{bmatrix} c \\ \rho/r \end{bmatrix}$ represents a point on the line of CORs (dual line of friction cone) in body frame.

Following similar steps in section 3.2.1, we can map the flat outputs to cartesian pose and applied force:

$$\theta = \arctan(\frac{-\dot{z}_1}{\dot{z}_2}) \tag{31}$$

$$\begin{bmatrix} x \\ y \end{bmatrix} = \begin{bmatrix} z_1 \\ z_2 \end{bmatrix} - \frac{1}{\sqrt{\dot{z}_1^2 + \dot{z}_2^2}} \begin{bmatrix} \dot{z}_2 & \dot{z}_1 \\ -\dot{z}_1 & \dot{z}_2 \end{bmatrix} \begin{bmatrix} c \\ \rho/r \end{bmatrix} \tag{32}$$

$$\begin{bmatrix} f_x \\ f_y \end{bmatrix} = \frac{1}{\dot{z}_1^2 + \dot{z}_2^2} \begin{bmatrix} \frac{\dot{z}_1 \ddot{z}_2 - \ddot{z}_1 \dot{z}_2}{br} \\ \frac{(\dot{z}_1^2 + \dot{z}_2^2)^{\frac{3}{2}} - c(\dot{z}_1^2 + \dot{z}_2^2)}{a} \end{bmatrix}. \tag{33}$$

Further, let c_l and c_r be the x components of the CORs corresponding to $\mathbf{f_l}$ and $\mathbf{f_r}$. If we set $c = (c_l + c_r)/2$, then the friction cone constraint is turned into a curvature upper bound of $2/|c_l - c_r|$ (or minimum turning radius of $|c_l - c_r|/2$.) We refer the readers to the appendix for detailed derivation.

4 Stabilization

Uncertainty for robotic pushing mainly come from two sources: 1) perception uncertainty for the initial object pose and 2) model uncertainty due to changing friction distribution. Single contact pushing cannot be open-loop stable and needs active feedback control strategy. Section 4.1 derives a linear tracking controller in flat output space through dynamic feedback linearization. Section 4.2 addresses improving robustness against model uncertainty through open-loop stable two-points push that naturally induces mechanical feedback.

4.1 Dynamic Feedback Linearization Control

Equation 12 is in the form of driftless underactuated system with three degrees of freedom state and two degrees of freedom control input:

$$\dot{\mathbf{q}} = G(\mathbf{q})\mathbf{f}. \tag{34}$$

For such systems, dynamic feedback linearization finds a feedback compensator of the form:

$$\dot{\zeta} = \alpha(\mathbf{q}, \zeta) + \beta(\mathbf{q}, \zeta)\mathbf{w} \tag{35}$$
$$\mathbf{f} = \gamma(\mathbf{q}, \zeta) + \delta(\mathbf{q}, \zeta)\mathbf{w}, \tag{36}$$

where the kth derivative of flat output z can be directly controllable via w

$$z^k = w. \tag{37}$$

Differentiating the flat output z with respect to time yields

$$\dot{z} = \begin{bmatrix} 0 & -a\sin\theta \\ 0 & a\cos\theta \end{bmatrix} \begin{bmatrix} f_x \\ f_y \end{bmatrix}. \tag{38}$$

We need to keep taking derivative since only f_y affects $\dot{z}$. Denote by $\zeta = f_y$ the dynamic feedback compensator and $s = \dot{\zeta}$.

$$\ddot{z} = a \begin{bmatrix} -\sin\theta & -\zeta br\cos\theta \\ \cos\theta & -\zeta br\sin\theta \end{bmatrix} \begin{bmatrix} s \\ f_x \end{bmatrix} \tag{39}$$

Let

$$\begin{bmatrix} s \\ f_x \end{bmatrix} = (a \begin{bmatrix} -\sin\theta & -\cos\theta \\ \cos\theta & -\sin\theta \end{bmatrix} \begin{bmatrix} 1 & 0 \\ 0 & \zeta br \end{bmatrix})^{-1} \begin{bmatrix} w_1 \\ w_2 \end{bmatrix} \tag{40}$$

$$= \begin{bmatrix} -\sin\theta/a & \cos\theta/a \\ -\cos\theta/(a\zeta br) & -\sin\theta/(a\zeta br) \end{bmatrix} \begin{bmatrix} w_1 \\ w_2 \end{bmatrix}, \tag{41}$$

which leads to

$$\ddot{z} = \begin{bmatrix} w_1 \\ w_2 \end{bmatrix} = w \tag{42}$$

The dynamic feedback compensator is of the following form:

$$\dot{\zeta} = -w_1\sin\theta/a + w_2\cos\theta/a \tag{43}$$

$$f_y = \zeta \tag{44}$$

$$f_x = -w_1\cos\theta/(a\zeta br) - w_2\sin\theta/(a\zeta br) \tag{45}$$

We can therefore design a simple PD controller to track a planned trajectory $z_d(t)$.

$$w = \ddot{z}_d - k_p(z - z_d) - k_d(\dot{z} - \dot{z}_d). \tag{46}$$

This PD controller is globally exponentially stable assuming the model does not change. A robustness analysis for a changing model is beyond the scope of this paper. The manipulator velocity control input can be further determined via equations 13 and 43-45.

A simulation experiment using a high-fidelity simulator [26] is shown in Figure 4b. The initial state is perturbed by -1mm in x, -2.5mm in y and 3.6 degrees in θ. The system model parameter A in equation 12 is perturbed from $\begin{bmatrix} 1.0537 & 0 & 0 \\ 0 & 1.0537 & 0 \\ 0 & 0 & 1.5087 \end{bmatrix}$ to $\begin{bmatrix} 1.0719 & -0.0177 & -0.1782 \\ -0.0177 & 1.0417 & 0.1599 \\ -0.1782 & 0.1599 & 1.5104 \end{bmatrix}$. The gain for position error term is $k_p = [2.0, 0.5]$ and the gain for velocity error term is $k_v = [0.1, 0.05]$. The controller runs at 60Hz for 30 seconds and the final pose error is 0.0034mm in x, 0.0012mm in y and 2.55 degrees in θ. The ABB robot is currently not suitable for closed-loop control due to low position control input frequency. In the future, we will conduct robotic experiments with recently released externally guided motion package [1].
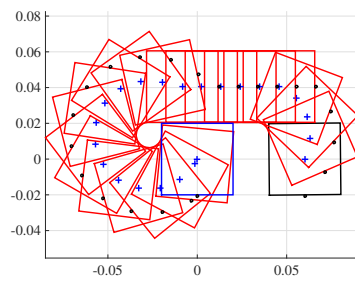
(a) Planned reference trajectory.
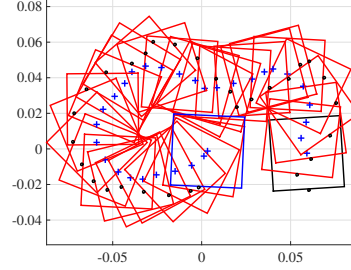
(b) Trajectory tracking with dynamic feedback linearization.

4.2 Open Loop Stabilization With Kinematic Constraints

Lynch and Mason [17] showed that a two-points push action against an edge of the object can be stable such that the object will remain attached to the pusher without slipping or breaking contact, despite the presence of uncertainty. This can be seen as natural mechanical feedback that tolerates model uncertainty. The object will follow a body twist motion $\mathbf{V}$ as long as the corresponding frictional wrench $\mathbf{F}$ is inside the composite wrench cone $F_c = \mathcal{K}(F_c^1, F_c^2)$ formed by the two wrench cones F_c^1, F_c^2 at the contact points, i.e., $\exists \mathbf{F}$ such that $\nabla H(\mathbf{F}) = \mathbf{V}$ and $\mathbf{F} \in \mathbf{F_c}$. The span of the composite wrench cone provides redundancy to balance uncertain frictional wrench between the object and the supporting surface.

Throughout our experiments, we use the mid point of the two points as a virtual contact point and the average normal as the contact normal to plan reference trajectory. Perception uncertainty is not addressed for this form of mechanical feedback although a sequence of designed open-loop translational pushes can reduce the initial perception uncertainty [3].

5 Experiments

5.1 Pushing using Multiple Actions

A pushing point in the body frame defines an action associated with a Dubins car reduction. If we allow switching between multiple pushing points (actions), the object can be moved faster to the goal state. It is also natural to specify a switching cost between actions. This section presents a simple planner that gives the near-optimal path for a given query initial pose to the goal pose at the origin. We first construct a graph using the following steps:
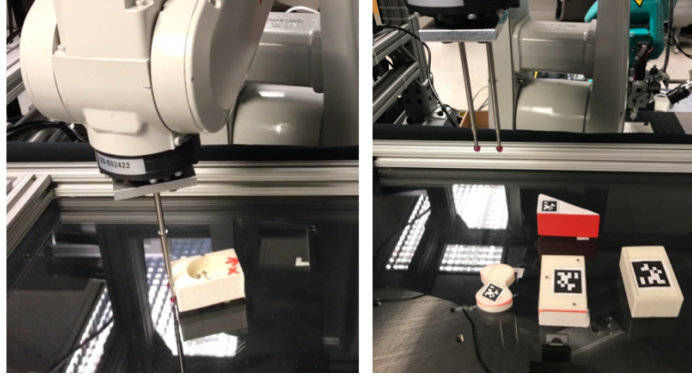
1. Sample SE(2) poses within the boundary as graph nodes.

Fig. 5: Experimental setup.

2. For each node, split into k copies tagged with action id, where k equals the number of actions.
3. Run Dijkstra's algorithm [5] and add switching cost to the edge weight if the two nodes are tagged with different action ids.

The graph is organized as a tree structure whose paths to the goal are the shortest path subject to the sampling resolution. Then for any new query pose, we treat it as a new node to connect to the goal through either direct connection to the goal using one action or paths in the graph using multiple actions.

The experimental setup is shown in Figure 5. We use the ABB-120 robot mounted with a two-points pusher. The object bottoms are attached with AprilTags [20]. The supporting surface is a transparent acrylic table with a camera underneath to acquire the initial and final poses. We use four objects with different pressure distributions, material and shapes. Trajectories are generated using the mid point of the two points as a single point pusher and executed open-loop. Each object is given three or four pushing points (actions). The triangular object has actions of asymmetric push point. Three different initial locations that require difficult maneuvers are chosen for each object with the same target location such that the local frame exactly aligns with table frame at the center. Each initial condition is executed five times. Trajectories generated from experimental logs are shown in Figure 6 to 9. The object initial poses (in sequence) for each action are filled with red, purple and blue colors. The final pose is filled with black color. The average error is within 1.67mm in translation and 0.5 degrees in orientation over the 60 experiments[1].

---

[1] All 60 runs videos are available at `https://www.dropbox.com/sh/2t6cwqwv3w95iji/AABLHdlnRhSQzHKhcmg2zOT4a?dl=0`.
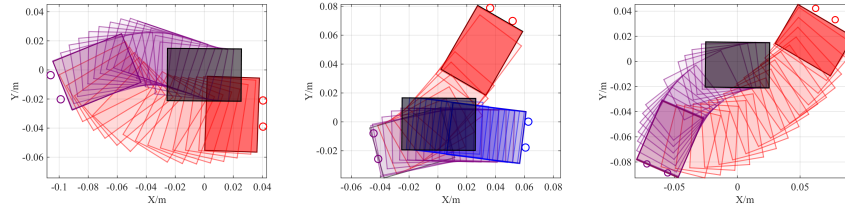
Fig. 6: Rectangle with three-point pressure. The average error (mm, mm, degree) with 95% confidence interval from left to right are $[0.03 \pm 0.02, -3.19 \pm 0.29, 0.53 \pm 0.11], [0.50 \pm 0.13, -0.96 \pm 0.6, -0.48 \pm 0.61], [-0.23 \pm 0.11, -4.17 \pm 0.87, -1.29 \pm 0.5]$.
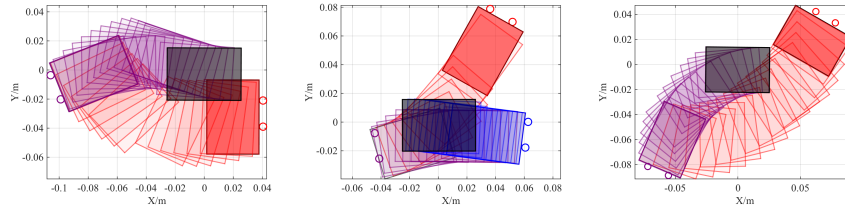

Fig. 7: Rectangle with boundary pressure. The average error (mm, mm, degree) with 95% confidence interval from left to right are $[-0.26 \pm 0.12, -3.31 \pm 0.75, -0.46 \pm 0.19], [0.42 \pm 0.12, -1.49 \pm 1.63, -0.14 \pm 0.27], [-0.27 \pm 0.21, -4.56 \pm 0.43, -0.93 \pm 0.76]$.
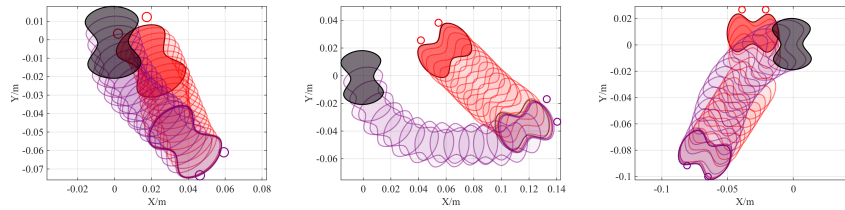

Fig. 8: The butterfly object with boundary pressure. The average error (mm, mm, degree) with 95% confidence interval from left to right are $[-0.69 \pm 0.17, -1.46 \pm 0.06, 4.40 \pm 1.24], [-0.65 \pm 0.17, -1.38 \pm 0.07, 5.89 \pm 2.37], [-0.96 \pm 0.08, -0.09 \pm 0.73, 0.83 \pm 1.00]$.

5.2 Pushing Among Obstacles

The proposed reduction to Dubins curve benefits randomized motion planners since the two point boundary value problem can be solved exactly via the reduction, i.e., the steering is exact. We use a RRT [15] planner to generate a collision free pushing path shown in Figure 10 and 11. The triangular object and the two-points pusher are not allowed to touch the red obstacle nor the blue boundary of the map. The goal is to align the center of the triangle with the red point in an up-right orientation.
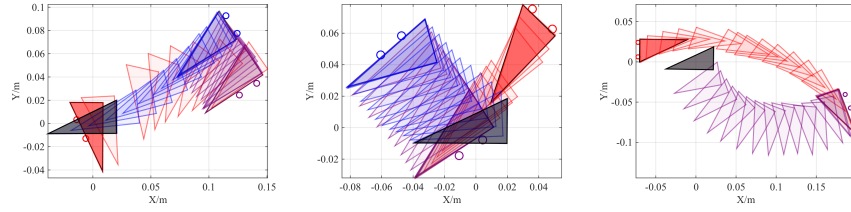
Fig. 9: Triangle with uniform pressure. The final error (mm, mm, degree) with 95% confidence interval are $[0.64 \pm 0.05, 1.04 \pm 0.63, 0.11 \pm 0.31], [0.11 \pm 0.65, -0.50 \pm 0.30, -0.42 \pm 0.44], [2.34 \pm 0.23, 0.12 \pm 0.06, -1.06 \pm 0.42]$.
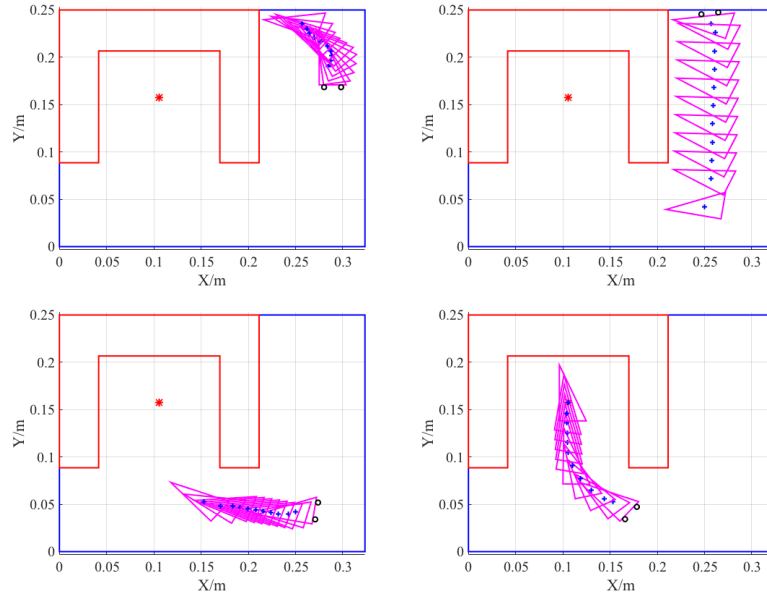

Fig. 10: Planned pushing actions among obstacles using RRT with exact steering.

6 Conclusions and Future Work

This paper studies the geometrical structure for the pusher-slider system with one rolling/sticking constraint: there exists body-fixed point whose trajectory completely determines the system behavior. Planning and control in this differentially flat (carefully chosen reduced minimal coordinates) space is significantly easier. In the future, we plan to conduct robotic experiments for the dynamic feedback linearization control with single point contact in a receding horizon fashion since unexpected slip may occur and the control needs to reveal the change of contact positions. Extension to three-dimensional space where out-of-plane moments cannot be neglected remains as a challenging problem.
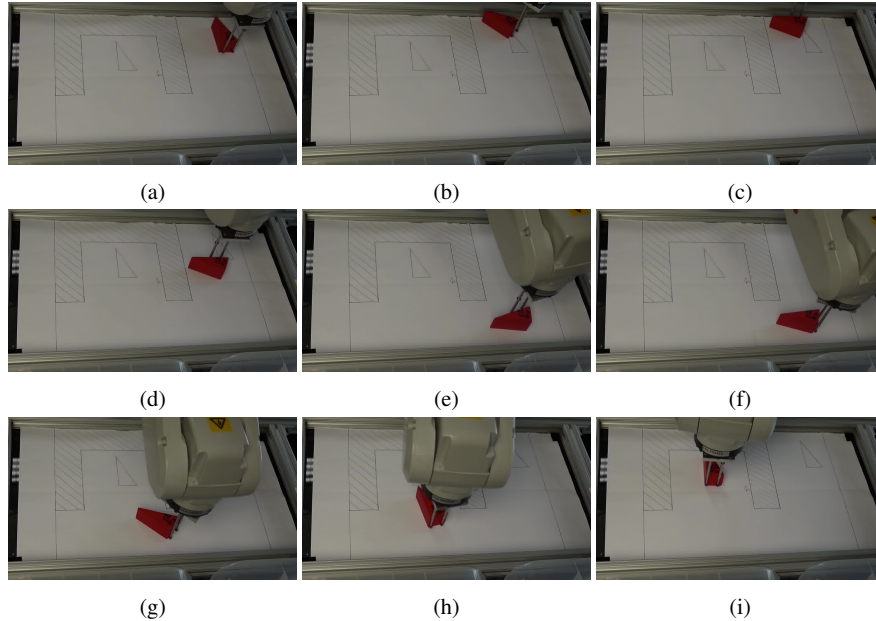
Fig. 11: Snapshots of the robot executing the plan.

References

1. ABB. Abb externally guided motion (egm).
   `http://new.abb.com/products/ABB.PARTS.SEROP3HAC054376-001`, 2017.
   [Online; accessed 14-June-2017].
2. Maria Bauza and Alberto Rodriguez. A probabilistic data-driven model for planar pushing.
   arXiv preprint arXiv:1704.03033, 2017.
3. Randy C Brost. Automatic grasp planning in the presence of uncertainty. *The International Journal of Robotics Research*, 7(1):3–17, 1988.
4. Randy C Brost and Matthew T Mason. Graphical analysis of planar rigid-body dynamics with multiple frictional contacts. In *The fifth international symposium on Robotics research*, pages 293–300. MIT Press, 1991.
5. Edsger W Dijkstra. A note on two problems in connexion with graphs. *Numerische mathematik*, 1(1):269–271, 1959.
6. Mehmet R Dogar and Siddhartha S Srinivasa. Push-grasping with dexterous hands: Mechanics and a method. In *Intelligent Robots and Systems (IROS), 2010 IEEE/RSJ International Conference on*, pages 2123–2130. IEEE, 2010.
7. Lester E Dubins. On curves of minimal length with a constraint on average curvature, and with prescribed initial and terminal positions and tangents. *American Journal of mathematics*, 79(3):497–516, 1957.
8. Kennneth Goldberg and Matthew T. Mason. Bayesian grasping. *IEEE International Conference on Robotics and Automation (ICRA)*, pages 1264–1269, 1990.

9. Suresh Goyal. *Planar Sliding of a Rigid Body With Dry Friction: Limit Surfaces and Dynamics of Motion*. PhD thesis, Cornell University, Dept. of Mechanical Engineering, 1989.

10. Suresh Goyal, Andy Ruina, and Jim Papadopoulos. Planar sliding with dry friction. Part 1. Limit surface and moment function. *Wear*, 143:307–330, 1991.

11. François Robert Hogan and Alberto Rodriguez. Feedback control of the pusher-slider system: A story of hybrid and underactuated contact dynamics. *arXiv preprint arXiv:1611.08268*, 2016.

12. Robert D Howe and Mark R Cutkosky. Practical force-motion models for sliding manipulation. *IJRR*, 15(6):557–572, 1996.

13. Eric Huang, Ankit Bhatia, Byron Boots, and Matthew T Mason. Exact bounds on the contact driven motion of a sliding object, with applications to robotic pulling. In *Robotics: Science and systems XIII*, 2017.

14. Steven M LaValle. *Planning algorithms*. Cambridge university press, 2006.

15. Steven M LaValle and James J Kuffner Jr. Randomized kinodynamic planning. *The international journal of robotics research*, 20(5):378–400, 2001.

16. Kevin M Lynch, Hitoshi Maekawa, and Kazuo Tanie. Manipulation and active sensing by pushing using tactile feedback. In *IROS*, pages 416–421, 1992.

17. Kevin M. Lynch and Matthew T. Mason. Stable pushing: Mechanics, controllability, and planning. *IJRR*, 15(6):533–556, December 1996.

18. Matthew T. Mason. Mechanics and planning of manipulator pushing operations. *IJRR*, 5(3):53–71, Fall 1986.

19. Richard M Murray, Muruhan Rathinam, and Willem Sluis. Differential flatness of mechanical control systems: A catalog of prototype systems. In *ASME international mechanical engineering congress and exposition*, 1995.

20. Edwin Olson. Apriltag: A robust and flexible visual fiducial system. In *Robotics and Automation (ICRA), 2011 IEEE International Conference on*, pages 3400–3407. IEEE, 2011.

21. Giuseppe Oriolo, Alessandro De Luca, and Marilena Vendittelli. Wmr control via dynamic feedback linearization: design, implementation, and experimental validation. *IEEE Transactions on control systems technology*, 10(6):835–852, 2002.

22. Michael A. Peshkin and Arthur C. Sanderson. Planning robotic manipulation strategies for workpieces that slide. 4(5):524–531, October 1988.

23. Michael Posa, Cecilia Cantu, and Russ Tedrake. A direct method for trajectory optimization of rigid bodies through contact. *The International Journal of Robotics Research*, 33(1):69–81, 2014.

24. Michael Posa, Scott Kuindersma, and Russ Tedrake. Optimization and stabilization of trajectories for constrained dynamical systems. In *Robotics and Automation (ICRA), 2016 IEEE International Conference on*, pages 1366–1373. IEEE, 2016.

25. J Wiegley, K Goldberg, M Peshkin, and M Brokowski. A complete algorithm for designing passive fences to orient parts. In *Robotics and Automation, 1996. Proceedings., 1996 IEEE International Conference on*, volume 2, pages 1133–1139. IEEE, 1996.

26. Jiaji Zhou, J Andrew Bagnell, and Matthew T Mason. A fast stochastic contact model for planar pushing and grasping: Theory and experimental validation. In *Robotics: Science and systems XIII*, 2017.

27. Jiaji Zhou, R. Paolini, J. A. Bagnell, and M. T. Mason. A convex polynomial force-motion model for planar sliding: identification and application. In *2016 IEEE International Conference on Robotics and Automation (ICRA)*, pages 372–377, May 2016.

28. Jiaji Zhou, R. Paolini, A. Johnson, J. A. Bagnell, and M. T. Mason. A probabilistic planning framework for planar grasping under uncertainty. In *Intelligent Robots and Systems (IROS), 2017 IEEE/RSJ International Conference on*, 2017.